Algorithm for Automatic Quantification of Flashback and Flash Forward Events from High-Speed Chemiluminescence Recordings

Robert-Zoltán Szász, Arman Ahmed Subash, Andreas Lantz, Robert Collin, Laszlo Fuchs and Ephraim J. Gutmark

Abstract Three methods are employed to identify and quantify flashback and flash forward events based on chemiluminescence recordings of swirling flames. The approaches differ in the procedure to determine the instantaneous flame position. The results revealed that the most robust method is to determine a threshold relative to the instantaneous maximum intensity. Analysis of the complete dataset indicated that flashback events are significantly slower than flash forward events.

1 Introduction

The current trend in gas turbine development is to improve fuel flexibility. The use of a wider variety of fuels, however, has impact on the reliability of the gas turbine. The increased span of fuel properties may lead to the appearance of flame instability issues. Such issues are flashback and blow-out, intensively studied in the literature (see e.g. [1–5]). In order to avoid the occurrence of flashback and blow-out, beside determining the safe working intervals for different fuels, one has to understand the dynamics of such events.

High speed recording of the chemiluminescence signal during flashback or blow-out is a relatively easy method to collect data which can help understanding the flame dynamics. Due to the large number of parameters one commonly needs to consider, such measurement campaigns often result in a large number of recordings leading to a need for automatic processing of the collected datasets. Such automatization is

R.-Z. Szász (✉)
Department of Energy Sciences, Lund University, PO.Box 118, 22100 Lund, Sweden
e-mail: robert-zoltan.szasz@energy.lth.se

A.A. Subash · A. Lantz · R. Collin
Department of Physics, Lund University, Lund, Sweden

L. Fuchs
Department of Mechanics, Royal Institute of Technology, Stockholm, Sweden

E.J. Gutmark
Department of Aerospace Engineering, University of Cincinnati, Cincinnati, USA

A. Segalini (ed.), *Proceedings of the 5th International Conference on Jets, Wakes and Separated Flows (ICJWSF2015)*,
Springer Proceedings in Physics 185, DOI 10.1007/978-3-319-30602-5_64

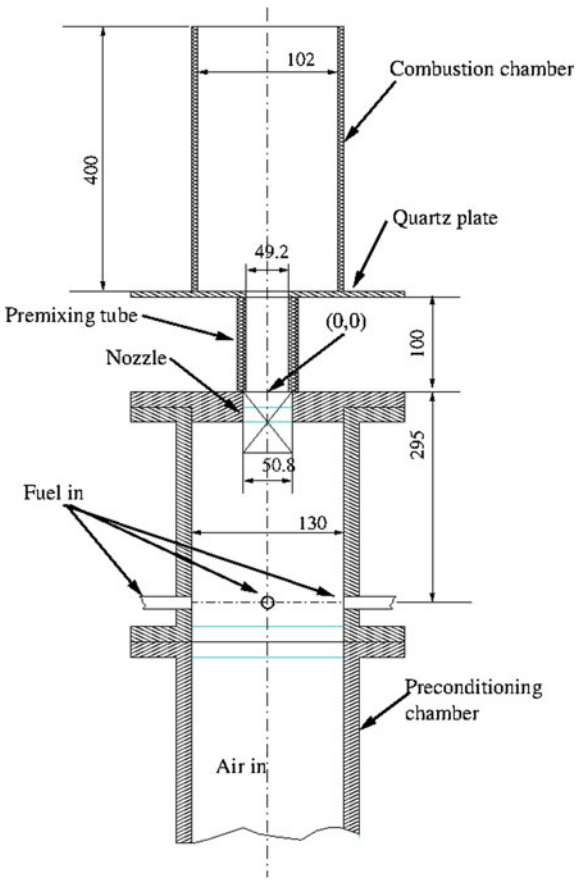

Fig. 1 Experimental rig

preferred also in order to obtain consistent postprocessing across datasets and avoid the often subjective human decisions. Here we propose such a method to postprocess high-speed chemiluminescence recordings.

2 Experimental Procedure

Figure 1 shows the experimental rig. Methane is premixed with air in a preconditioning chamber. The mixture passes through three co-annular swirlers into a quartz premixing tube having a length of two tube diameters. Above the premixing tube a quartz plate and a quartz combustion chamber are mounted. In the present paper, flash-forward denotes the propagation of the flame from the premixing tube into the combustion chamber.

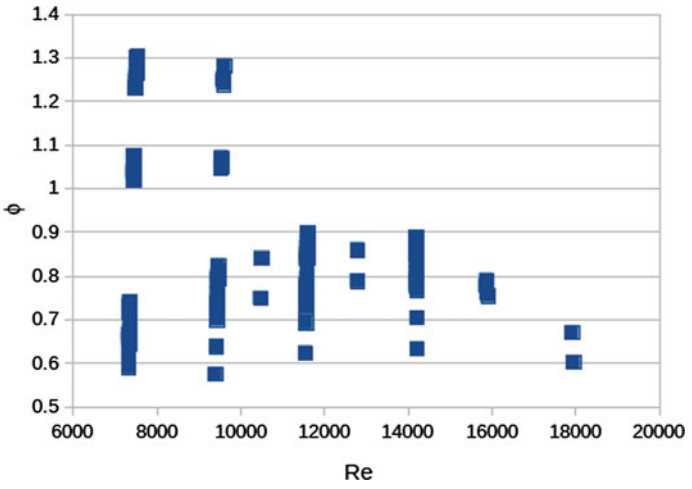

Fig. 2 Reynolds number and equivalence ratio ranges studied in the experiments

For combustion applications one of the important parameters controlling the flame is the fuel-air ratio, *FAR*, defined as the ratio of the fuel and air mass flow rates (see (1)).

$$FAR = \frac{\dot{m}_F}{\dot{m}_A} \tag{1}$$

The equivalence ratio, ϕ, is the actual fuel-air ratio normalized with the fuel-air ratio in stoichiometric conditions (2). Thus, equivalence ratio values smaller then unity indicate lean conditions (i.e. there is more oxidizer available than needed by the fuel), whereas values larger than one correspond to rich conditions, when fuel is in excess.

$$\phi = \frac{FAR}{FAR_{st}} \tag{2}$$

During the measurements the Reynolds number was fixed to prescribed values and the equivalence ratio interval was scanned, by altering the fuel flow rate, from very lean to very rich conditions to trigger flashback or flash forward events. Figure 2 shows a scatter plot of the Reynolds number and equivalence ratio ranges covered in the experiments.

A high speed video camera (Phantom V7.1, Vision Research) was used to record the chemiluminescence signal from the flame. The camera features an 800 × 600 pixel SR-CMOS monochromatic sensor and has a repetition rate of 4.8 kHz at full resolution. The camera was equipped with a gated image-intensifier (Hamamatsu) in order to enhance its sensitivity and a UV sensitive camera lens (UV-Nikkor, f/2.5, f = 105 mm). To capture the flashback and flash forward events a recording rate of 1 kHz was used, pre-triggering 1000 samples, the total number of samples being 1200. Both the premixing tube and part of the combustion chamber have been recorded to be able to follow the flame front during flashback or flash forward.

3 Post Processing Method

The method was tested on the database consisting of 260 videos obtained by varying several flow parameters. The algorithm consists of three stages, schematically visualized on the block diagram in Fig. 3. In the block diagram ellipses mark input/output data and rectangles denote processing stages of the algorithm.

First, the intensity of the chemiluminescence frames is integrated along radial lines resulting in an intensity vector for each time instance. Let $I(x, y, t)$ denote the intensity of an image recorded at time instance t and horizontal and vertical positions x and y, respectively. Furthermore, N_x and N_y are the number of pixels in horizontal and vertical directions, whereas N_t is the number of recorded frames. The integrated intensity vector is then computed using (3).

$$II(y, t) = \sum_{x=1}^{N_x} I(x, y, t) \tag{3}$$

Figure 4 shows the time evolution of these intensity vectors for a flash forward event (top) and a flashback event (bottom). The dark horizontal line in the middle of the image is due to the quartz plate separating the premixing tube from the combustion chamber.

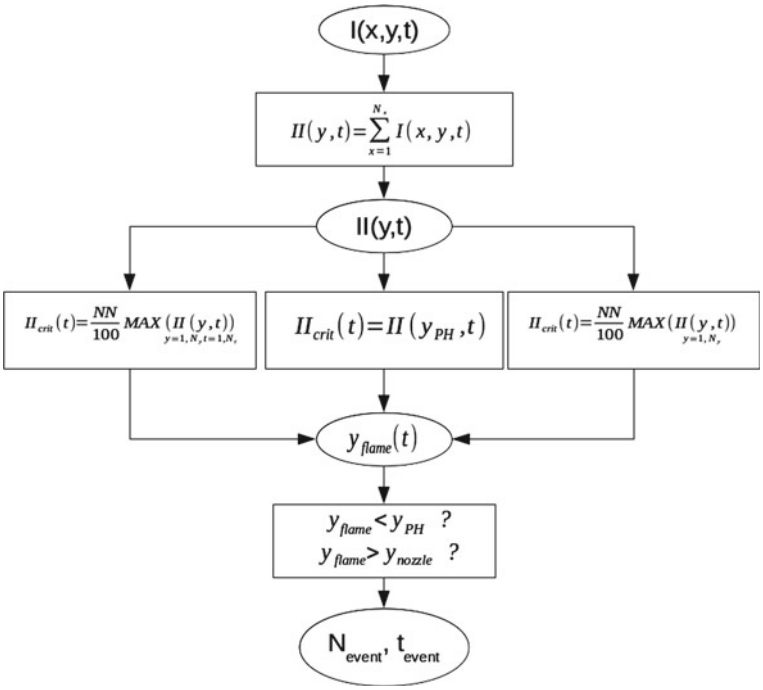

Fig. 3 Block diagram of the post-processing method

In the second stage the flame position is determined. For each time instance, beginning at the lowest position (close to the nozzle) and moving towards the combustion chamber, the integrated intensity values are compared to a critical value. It is assumed that the flame is located where this critical value is first exceeded, $II(y,t) > II_{crit}$. Since the intensity at the flame position depends on the equivalence ratio, the idea of using a fixed threshold for the whole database was discarded. Three types of thresholds were tested:

1. The first method is based on the idea to set the critical pixel intensity as a certain percentage of the maximum pixel intensity during an entire recording, $II_{crit} = NN/100 \cdot MAX(II(y,t))_{\forall y,\forall t}$. These cases are denoted as TI*NN* in the followings, *NN* being the critical threshold (in %). A larger value of *NN* results thus in a larger value of the critical intensity and the predicted flame position is expected to be located at higher vertical positions, closer to the lighter areas of the intensity-integrated images.
2. Since the quartz plate separating the premixing tube from the combustion chamber generates a shadow in the images, regions with larger intensities than in this region can be regarded as flame locations. When the flame flashes back (or forward), the areas in the vicinity of the plate shadow must have a sudden change in intensity. Thus, in the second approach, the critical intensity value is set to the values located in the shadowed areas, $II_{crit}(t) = II(y_{PH}, t)$, y_{PH} being the vertical position of the quartz plate in the image. This method is denoted next as PH.
3. It was observed, that the intensity of the flame was varying in time even for constant air and fuel flow rate settings, thus different frames of a certain recorded sequence had different maximum intensity values. The third method to detect flame position is setting the threshold relative to the maximum intensity at a certain time instance, $II_{crit}(t) = NN/100 \cdot MAX(II(y,t))_{\forall y}$. These methods are denoted as L*NN*, where *NN* again denotes the percentage of the maximum intensity.

Eight tests have been carried out, three based on method 1, one based on method 2 and four based on method 3, these cases being summarized in Table 1. As one can conclude from the table, the optimal thresholds are 15 % total intensity and 30 % instantaneous snapshot intensity, leading to only 2 (in case TI15) and 1 (case L30) missed event out of the total of 260 flashback and flash-forward events. Both the lower and larger tested limits result in worse performance.

Figure 5 shows the time evolution of the flame tip position for the same cases as the ones shown in Fig. 4. For clarity, only the best performing test from each approach is shown. One can observe that the flame position in the TI15 and L30 cases are almost identical, especially in the flashback case, whereas the PH method detection is poor, the flashback event is detected for example as being much shorter and being followed by an unsuccessful flash forward event.

As a last step, based on the time evolution of the flame position relative to the quartz plate (incomplete and complete) flashback and flash forward events are identified and their parameters are quantified. Incomplete events are the ones that begin before a certain recording started or finish after the recording was stopped. By iden-

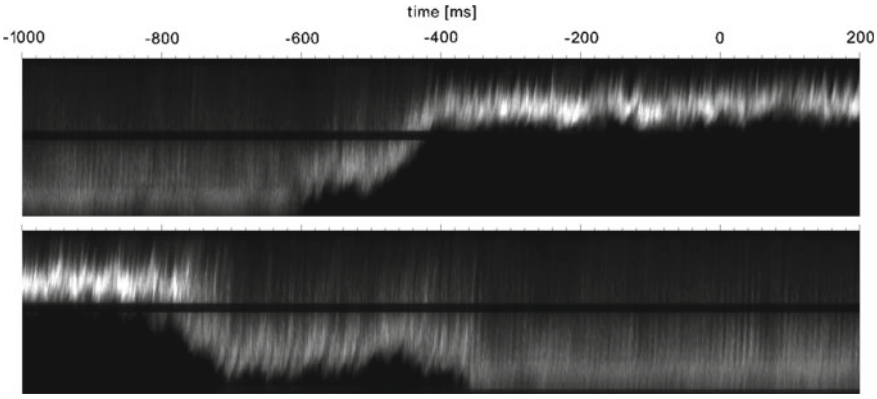

Fig. 4 Time evolution of the chemiluminescence intensity signal integrated along radial *lines*. Case with flash-forward (*top*) and flashback (*bottom*)

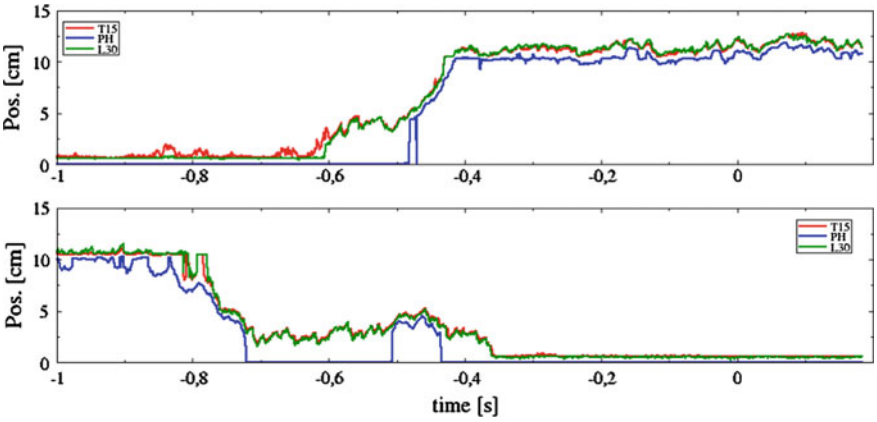

Fig. 5 Time evolution of the detected flame tip position. Case with flash-forward (*top*) and flashback (*bottom*)

tifying the time instances when the flame tip enters/leaves the premixing tube and when it attaches/detaches from the nozzle one can compute the duration of the phenomena and their average speed.

To check the accuracy of the detected durations, eight cases have been chosen out of the 260 recordings. The chosen cases were recorded for four flashback (denoted with FB1...FB4) and four flash forward events (denoted FF1...FF4). The duration of the events for the eight cases has been determined by visual analysis of the recordings and the predictions from the suggested methods have been compared to these values. Figure 6 shows the error (relative to the visually determined values) in the predicted event durations using the suggested approaches. Columns 3 and 4 of Table 1 shows the average and rms of the errors. Although the number of samples is small (eight)

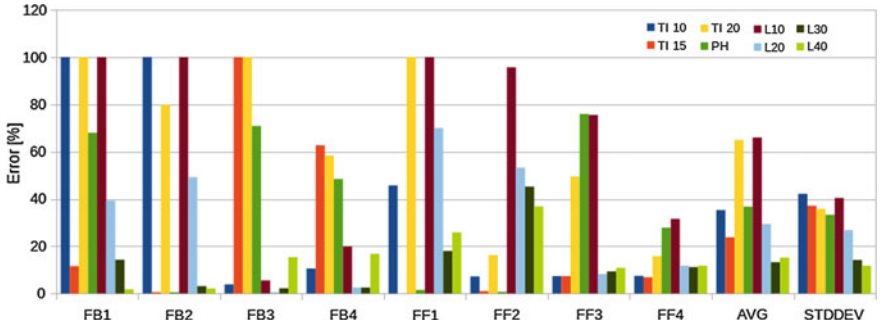

Fig. 6 The error in the event duration for four flashback (FB*X*) and flash forward (FF*X*) events. Average and RMS of the errors for the selected eight cases

Table 1 Summary of the methods

Method	Nr. missed	Avg. err. [%]	RMS err. [%]	Avg. flash-forward duration [s]	Avg. flashback duration [s]
TI10	12	35	42	0.145	0.291
TI15	2	24	37	0.201	0.291
TI20	14	65	36	0.124	0.381
PH	22	37	33	0.085	0.193
L10	19	66	40	0.107	0.225
L20	3	29	27	0.113	0.246
L30	1	13	14	0.114	0.247
L40	3	15	12	0.130	0.241

the results still provide information regarding the prediction quality of the suggested methods. One can observe that the L30 method results in the lowest error. Although L40 had one more missed event compared to TI15, it has smaller error in the prediction of the events' duration. It is also important to notice, that the methods based on the maximum intensity in an individual snapshot have generally lower fluctuations in the errors, thus they are expected to be more robust.

The average duration of all flashback events and all flash forward events were computed with the proposed approaches and are reported in the last two columns of Table 1. Since the 260 events accounted in the averaging cover a wide range of flow parameters (Reynolds number, equivalence ratio, combustor geometry, etc.) the averaged duration should not be interpreted physically. Nevertheless, important conclusions can be drawn from the results. As it regards the detection methods, one can conclude that the method based on the maximum intensity in a snapshot is the most robust. Changing the threshold from 10 to 40 % results in relatively small change in the predicted average duration of the events. The method based on the maximum intensity for a complete recording is much more sensitive, for 5 % change in the threshold the predicted average durations can change more than 25 %.

Another important conclusion is that flash-forward events are significantly faster than flashback events. Looking at Fig. 5 one can see that the slope of the flame position evolution in time is similar for flashback and flash forward when the flame is in the upper part of the premixing tube. Thus, one reason for the longer flashback duration might be stagnation of the flame front in the lower half of the premixing tube before a complete flashback occurs. However, experiments repeated for the same flow conditions revealed that the time evolution of the flame tip position can differ even for the same set-up, thus no conclusions should be drawn from individual events and more thorough analysis of the recorded data is necessary.

4 Conclusions

Methods have been suggested to automatically detect and quantify flashback and flash forward events from high-speed chemiluminescence videos of swirling flames. All suggested methods are divided in three stages. First, the intensity along radial lines has been integrated for each frame. Second, the flame tip position is determined by checking where this radially integrated intensity exceeds critical threshold. In the final stage the occurrence and duration of flashback or flash forward events is determined by identifying the time instances when the flame enters or leaves the premixing tube and attaches or detaches from the nozzle. The suggested methods differ in the second stage, three different ways of setting a critical threshold has been evaluated. The results show that the most robust method is to set the critical limit as a percentage of the maximum intensity of an individual frame. The statistics over the whole recorded dataset revealed that generally flashback events are significantly slower than flash forward events.

Acknowledgments The authors would like to acknowledge the support provided through the Center for Combustion Science and Technology, CECOST.

References

1. Y. Sommerer, D. Galley, T. Poinsot, S. Ducruix, F. Lacas, D. Veynante, J. Turbul. **5**(037) (2004)
2. J. Fritz, M. Kröner, T. Satt elmayer, J. Eng. Gas Turbines Power **126**(2), 276 (2004). doi:10.1115/1.1473155, http://link.aip.org/link/JETPEZ/v126/i2/p276/s1&Agg=doi
3. S.M. Hosseini, R.Z. Szasz, P. Iudiciani, L. Fuchs, A. Lantz, R. Collin, M. Aldén, E. Gutmark, in *46th AIAA/ASME/SAE/ASEE Joint Propulsion Conference & Exhibit* (2010), pp. 1–12
4. R. Lückerath, O. Lammel, M. Stöhr, I. Boxx, U. Stopper, W. Meier, B. Janus, B. Wegner, in *Proceedings Of The ASME Turbo Expo* (2011), GT2011–45790
5. C. Mayer, J. Sangl, T. Sattelmayer, T. Lachaux, S. Bernero, in *Proceedings Of The ASME Turbo Expo* (2011), GT2011–45125